JOURNAL OF GUIDANCE, CONTROL, AND DYNAMICS
Vol. 15, No. 4, July-August 1992

Spacecraft Dynamical Distribution of Fluid Stresses Activated by Gravity-Jitter-Induced Slosh Waves

R. J. Hung* and C. C. Lee†
University of Alabama in Huntsville, Huntsville, Alabama 35899
and
F. W. Leslie‡
NASA Marshall Space Flight Center, Huntsville, Alabama 35812

The dynamical behavior of fluids, in particular the effect of surface tension on partially filled rotating fluids (cryogenic liquid helium and helium vapor) in a full-scale Gravity Probe-B Spacecraft propellant Dewar tank imposed by various frequencies of gravity jitters, has been investigated. Fluid stress distribution, caused by the excitation of slosh waves and their associated large-amplitude disturbances on the liquid-vapor interface, exerted on the outer and inner walls of a rotating Dewar container also has been investigated. Results show that fluid stress distributions near the outer and inner walls of the rotating Dewar are closely related to the characteristics of slosh waves excited on the liquid-vapor interface in the rotating Dewar tank. This can provide a useful tool for managing spacecraft dynamic control leading toward the control of spacecraft imbalance caused by the uneven fluid stress distribution due to slosh wave excitations at the interface between liquid and vapor propellants.

I. Introduction

THE Gravity Probe-B (GP-B) Spacecraft is a relativity gyroscope experiment to test two extraordinary, unverified predictions of Einstein's general theory of relativity.[1,2] The experiment will check, very precisely, tiny changes in the direction of spin of four gyroscopes contained in an Earth satellite moving in a 650-km-altitude polar orbit. So free are the gyroscopes from disturbances that they will provide an almost perfect space-time reference system. They will measure how space and time are warped by the presence of the Earth and, more profoundly, how the Earth's rotation drags space-time around with it. These effects, though small for the Earth, have far-reaching applications for the nature of matter and the structure of the universe.

In the general theory of relativity, Einstein interpreted gravity not as a force but as a field distorting space and time. By using gyroscopes, the GP-B Spacecraft measures two distinct space-time processes, frame dragging (measuring the rotation of space-time) and the geodetic effect (measuring the curvature of space-time), that gradually change its direction of spin. In these gyroscopes, the underlying principle is that rotating systems, free from disturbing forces, should stay pointing in the same direction in space.

The physical meaning of "the same direction in space" can be explained from the differences in Newtonian and Einsteinian concepts of the universe. For Newton, the answer was easy: space and time were absolutes. A perfect gyroscope set spinning and pointed at a star would stay aligned forever. This was not so for Einstein. For Einstein, space and time were warped. A gyroscope orbiting the Earth would find the two distinct space-time processes, frame dragging and the geodetic effect, that will be measured by the GP-B.

Received Feb. 27, 1990; revision received July 17, 1991; accepted for publication Aug. 9, 1991.

*Professor of Mechanical Engineering. Associate Fellow AIAA.
†Staff Engineer.
‡Chief, Branch of Fluid Dynamics.

In order to ensure these extremely precise and accurate measurements and gyroscope operations, near-zero temperature practice is required for mechanical stability of the instrument, preservation of the lead bag magnetic shield shielding the gyroscopes against nongravitational disturbances, and of reading their direction of spin. Near-zero temperature cryogenic liquid helium II (1.8 K) is chosen to serve this purpose. The Dewar container is adopted to store gyroscopes and other key instruments, such as telescope, superconducting shields, drag-free proof mass, etc., in the core surrounded by the cryogenic liquid helium II (see Fig. 1).

The four gyros in the GP-B Spacecraft are used to monitor the rate of precession in free fall around the Earth. Extraneous forces on these gyros must be kept at very low levels, corresponding to an acceleration of $10^{-10}g_0$ ($g_0 = 9.81$ m/s^2) or less. This will require a drag-free (to $10^{-10}g_0$) control system that uses a proof mass similar to the experimental gyros as its sensing element. The experiment uses superconducting sensors for gyro readout and maintains very low temperature for mechanical stability. The approaches to both cooling and control involve the use of superfluid liquid helium. The boiloff from the cryogenic liquid helium Dewar (Fig. 1) will be used as a propellant to maintain the attitude control and drag-free translation of the spacecraft. The requirement for an operational lifetime approaching one year means that a large quantity of cryogenic liquid helium must be used and that the initially large mass of liquid helium will be gradually depleted over the lifetime of the experiment. This varying amount of liquid helium gives rise to the possibility of several problems that can degrade the GP-B experiment. Two potential problems are those due to asymmetry in the static liquid helium distribution or to perturbations in the free surface.

Cryogenic liquid helium II, at a temperature of 1.8 K, is used as the propellant for the GP-B Spacecraft. With its superconducting behavior, there is no temperature gradient in the liquid helium. In the absence of a temperature gradient along the surface to drive Marangoni convection, the equilibrium shape of free surface is governed by a balance of capillary, centrifugal, and gravitational forces. In contrasting the effects of surface tension with the effects of gravitational forces on the free surface of liquid, it was found that the surface tension force for most liquids is greater than the gravitational force of $10^{-8}g_0$.[3-5] In other words, the equi-

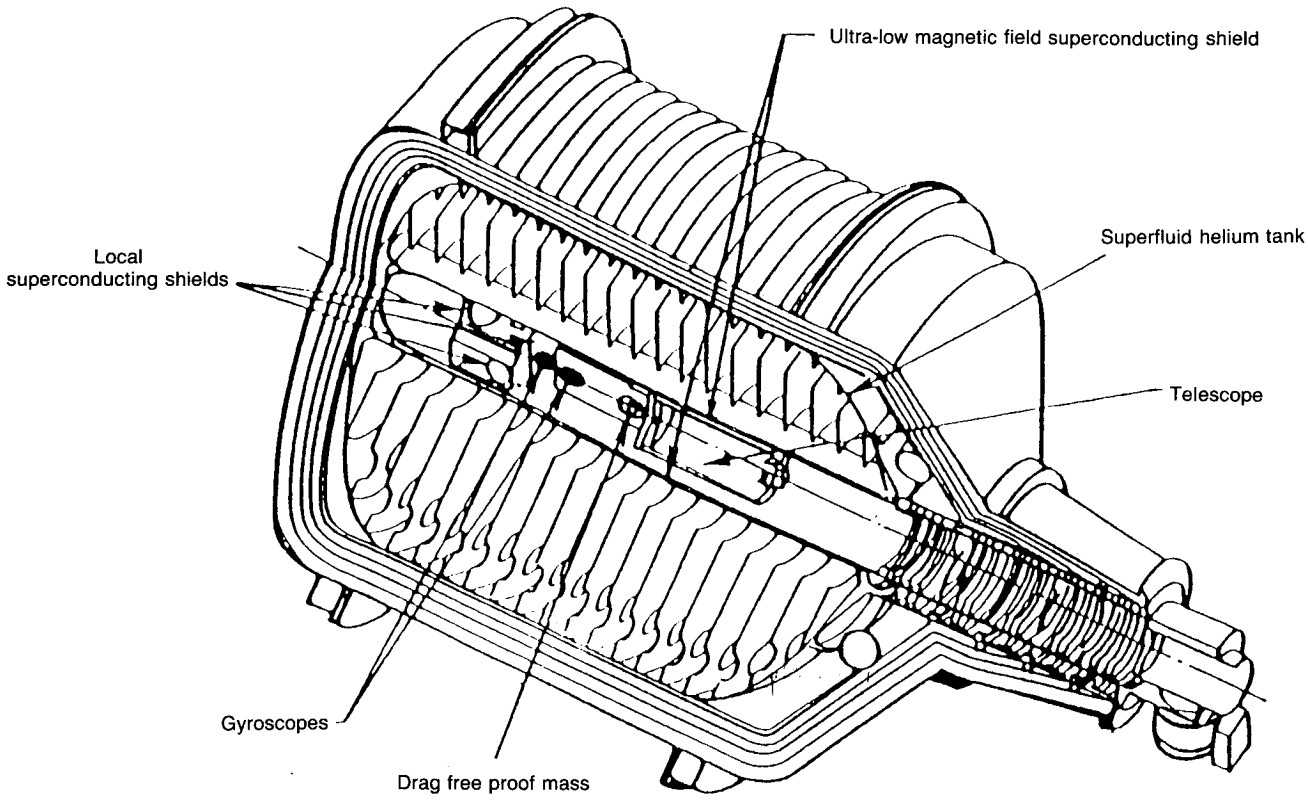

Fig. 1 Experiment Gravity Probe-B module showing main elements of liquid helium Dewar and probe.

librium shape of the liquid helium free surface in the operational GP-B Spacecraft is governed by a balance of capillary and centrifugal forces, instead of a balance of capillary, centrifugal, and gravitational forces. Therefore, one may ignore the effect of gravitational force in the gravity environment levels of $10^{-8}g_0$ and lower, in comparison to the surface tension force. Determination of vapor profiles based on computational experiments can uncover details of the flow that cannot be easily visualized or measured experimentally under a microgravity environment.[6-9]

Surface tension plays an important role in a large variety of fluid flows. The equilibrium shape of the free surface for the unsteady state rotating fluids is governed by the balance of capillary, bulk pressure, viscous, centrifugal, and gravity forces. The configuration of interface between liquid and gaseous fluids will be modified greatly when the gravity field reduces to microgravity levels. The instability of the liquid surface can be induced by the presence of longitudinal and lateral accelerations, vehicle vibration, and rotational forces of the spacecraft in a microgravity environment. Slosh waves are, thus, excited, which produces high- and low-frequency oscillations in the liquid propellant. The sources of the residual accelerations range from the effects of the Earth's gravity gradient, atmospheric drag on the spacecraft, and spacecraft attitude motions to the various frequency ranges of g-jitter arising from machinery vibrations, thruster firings, and crew motions. Recent research[10-12] suggests that the high-frequency accelerations may be unimportant in comparison to the residual motions caused by low-frequency accelerations.

Behavior of the liquid propellant becomes uncertain when the gravity environment is reduced to on the order of $10^{-6}g_0$. The requirement to settle or to position liquid fuel over the outlet end of the spacecraft propellant tank prior to main engine restart poses a significant microgravity fluid behavior problem. Retromaneuvers of spacecraft, such as the orbital maneuvering vehicle (OMV) and space transfer vehicle (STV)[13] during flight from high Earth orbit to low Earth orbit, will require settling or reorientation of the propellant prior to main engine firing. Usually cryogenic liquid propellant is positioned over the tank outlet by using small auxiliary thrusters (or idle-mode thrusters from the main engine), which provide a thrust parallel to the tank's major axis in the direction of flight.[14]

Time-dependent dynamical behavior of surface tension on partially filled rotating fluids in both low-gravity and microgravity environments has been carried out by numerically computing the Navier-Stokes equations subjected to the initial and the boundary conditions.[5,15-22] At the interface between the liquid and the gaseous fluids, both the kinematic surface boundary condition and the interface stress conditions for components tangential and normal to the interface were applied.[15-22] The initial condition of vapor profiles was adopted from the steady-state formulations in which the computer algorithms have been developed by Hung and Leslie[3] and Hung et al.[4] in a rotating cylinder tank; and also Hung et al.[4,16] in the coordinate of the Gravity Probe-B Spacecraft.[2] Some of the steady-state formulations of vapor shapes, in particular, for vapor intersecting the top wall of the cylinder, were compared with the available experiments carried out by Leslie[6] in a free-falling aircraft (KC-135). In the KC-135 experiments, the background gravity varies from 1.8 to $10^{-2}g_0$ during the 30-s low-gravity period. Accelerometer measurements are unavailable. However, comparisons of time-dependent results between numerical computations and experiments are not possible at this time. For the GP-B Spacecraft cryogenic liquid helium management problem, the geometries are so large that the critical values of a superfluid are exceeded. The experiments carried out by Mason et al.[23] showed that the classical fluid mechanics theory is applicable for cryogenic liquid helium in large containers.[23,24] The equilibrium configurations of the helium vapor in a rotating Dewar were studied.[4,16] They are relevant to the questions of fluid behavior in a microgravity environment that were raised by design and operational considerations for the GP-B experiment. For a spacecraft operating as designed, spacecraft drag will be balanced by the helium propulsion system. There should be no net acceleration, above the $10^{-10}g_0$ level, on the liquid helium from these sources. Our earlier studies[3-5] showed that the

gravitational force of $10^{-8}g_0$ level and lower will never affect the equilibrium shape of the liquid helium free surface because the effect of the surface tension force is overwhelmingly greater than that of the gravitational force at these levels.

As to the effect of centrifugal force on the liquid helium and helium vapor, the propellant tank will not be spinning when the GP-B Spacecraft is deployed. In the early stages of the experiment, a spin rate of up to about 1 rpm will be imposed for instrument calibration. After calibration, the rotation rate will be reduced to its operational value of approximately 0.1 rpm.

During the study described here, time-dependent computations were carried out to investigate the dynamical behaviors of cryogenic liquid helium and helium vapor in the geometry of a full-scale GP-B propellant Dewar container under a microgravity environment. The computations were also extended to study sloshing waves induced by the various frequencies of gravity jitters and variations in different rotating speeds of the GP-B Dewar container and different background gravitational fields. In this paper, slosh-wave-induced stress distributions on the external and internal walls of the propellant Dewar container are considered. This study will disclose time-dependent fluctuation in dynamical torque due to uneven viscous stress distributions that are initiated by the excitation of slosh waves propagating along the liquid-vapor interface. The large-amplitude oscillations of the liquid-vapor interface will enhance the fluctuations in moment of inertia of the rotating Dewar container, which causes the disturbances in angular momentum of the dynamical system of spacecraft. Understanding fluctuations of torque and angular momentum of spacecraft can provide a useful tool for spacecraft dynamic control, in particular, the attitude control of spacecraft dynamic imbalance caused by the uneven stress distributions due to the excitation of slosh waves that are induced by the oscillations at the liquid-vapor interface.

II. Dynamical Behavior of Liquid-Vapor Interface

Detailed descriptions of the time-dependent mathematical formulation, initial and boundary conditions, together with a computational algorithm applicable to cryogenic fluid management in a microgravity environment, are given in our earlier studies.[5,11,12,15-22] For this paper, a full-scale GP-B spacecraft propellant tank with a radius of 68 cm and a height of 145 cm was used in the numerical simulation. The propellant tank was 80% filled with cryogenic liquid helium and the rest of the ullage (20%) was filled with helium vapor. The temperature of cryogenic helium is 1.8 K. In this study, the following data were used: liquid helium density = 0.1457 g/cm^3, helium vapor density = 0.00147 g/cm^3, fluid pressure = 1.6625×10^4 dyne/cm^2, surface tension coefficient at the interface between liquid helium and helium vapor = 0.353 dyne/cm, liquid helium viscosity coefficient = 9.609×10^{-5} cm^2/s, and the contact angle = 5 deg. The initial profiles of the liquid-vapor interface for a rotating Dewar were determined from computations based on algorithms developed for the steady-state formulation of microgravity fluid management.[4,16]

A staggered grid for the velocity components is used in the computer program. This type of grid was developed by Harlow and Welch[25] for their MAC (marker and cell) method of studying fluid flows along a free surface. The finite difference method employed in this numerical study is the hybrid scheme developed by Spalding.[26] The formulation for this method is valid for any arbitrary interface location between the grid points and is not limited to middle point interfaces.[27] An algorithm for a semi-implicit method[27,28] was used as the procedure for modeling the flowfield. The time step is determined automatically based on the size of the grid points and the velocity of the flowfield. The computational algorithm applicable to microgravity fluid management is illustrated in our earlier studies.[5,11,12,14-22] Figure 2 shows the distribution of grid points for a Dewar tank in the radial-axial plane of cylindrical coordinates.

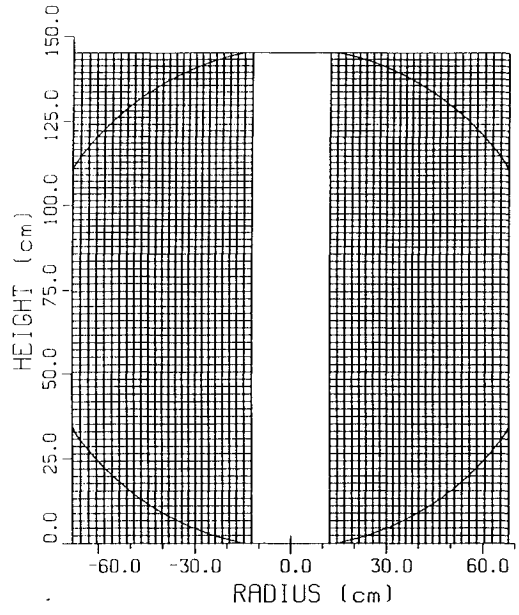

Fig. 2 Distribution of grid points in the radial axial plane of cylindrical coordinate for the propellant Dewar tank.

The most important computation in this study is the setting up of conditions between the vapor and liquid interface. At the interface, the stress must be continuous. These can be decomposed to the components normal and tangential to the interface. For the component tangential to the interface between liquid and vapor fields

$$[(\tau_{ij}t_in_j)]_{\text{liquid}} = [(\tau_{ij}t_in_j)]_{\text{vapor}} \tag{1}$$

must hold. Here,

$$\tau_{ij} = \mu\left(\frac{\partial u_i}{\partial x_j} + \frac{\partial u_j}{\partial x_i} + \frac{2}{3}\frac{\partial u_k}{\partial x_k}\delta_{ij}\right) + \zeta\frac{\partial u_k}{\partial x_k}\delta_{ij}$$

is the viscous stress tensor, μ the viscous coefficient of the first kind, ζ the viscous coefficient of the second kind, t_i the unit vector tangential to the interface, n_j the unit vector normal to the interface, u_i the flow velocity, and δ_{ij} the Dirac delta function. For the component normal to the interface between the liquid and gaseous fluids, the expression becomes Laplace's formula, which is

$$P_G - P_L - (\tau_{ij}n_in_j)_{\text{vapor}} + (\tau_{ij}n_in_j)_{\text{liquid}} = -\frac{\sigma}{r}\frac{\mathrm{d}}{\mathrm{d}r}\left[\frac{r\psi}{(1+\psi^2)^{1/2}}\right] \tag{2}$$

Here, P_L denotes the liquid pressure at the interface, P_G the gaseous pressure at the interface, σ the surface tension of the interface, and ψ the tangent of the interface, which is defined by

$$\psi = \frac{\mathrm{d}z}{\mathrm{d}r} \quad \text{on} \quad \eta_i = \eta(t_i, r, z) \tag{3}$$

Gravity jitters are the fluctuations of gravity fields and gravity gradients that are particularly pronounced in a low-gravity environment. Under a microgravity environment, gravity jitters are produced by spacecraft attitude motion, space environment fluctuations in density distribution, spacecraft machinery (turbine, pump, engine, etc.) vibrations, thruster firing, thruster shutdown, etc.[10-12,14,17,19-22] Vibration of the gravity environment (gravity jitters) is governed by the follow-

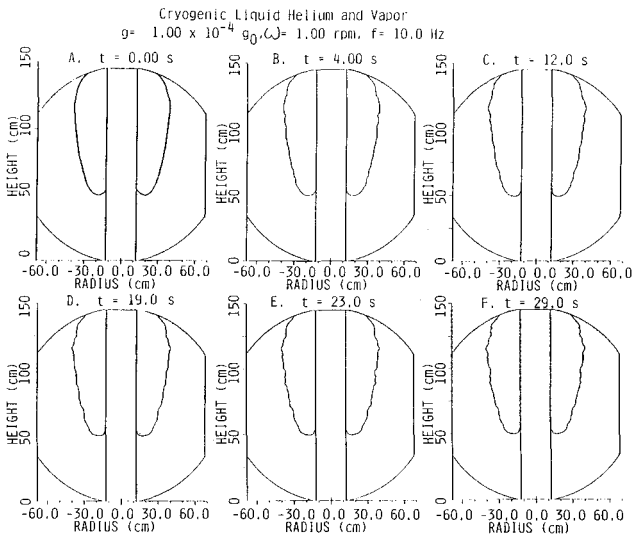

Fig. 3 Time sequence of dynamical evolutions for interface oscillations between liquid helium and helium vapor under background gravity environment of $10^{-4}g_0$, rotating speed of 1.0 rpm, and gravity jitter frequency of 10.0 Hz. The sequence shows slosh wave evolution at different time periods from 0.0 to 29.0 s.

ing equation:

$$g = g_B[1 + \tfrac{1}{2} \sin (2\pi ft)] \tag{4}$$

where g_B denotes the background gravity environment, and f (Hz) is the frequency of the gravity jitters.

The equilibrium shape of the liquid-vapor interface for a rotating Dewar under a background gravity environment of $10^{-4}g_0$ and rotating speed of 1.0 rpm is a vertically elongated doughnut with a near conical shape cross section based on the computation of the numerical algorithm developed in our earlier studies.[4,16] Figure 3 shows the time sequence evolution of the dynamical behaviors of the liquid-vapor interface oscillations driven by the restoring force fields of gravity jitters with a frequency of 10 Hz. In this condition, the elongated doughnut shape configuration of the liquid-vapor interface is attached to the top wall of the Dewar.

It shows clearly that both horizontally and vertically propagated transverse and longitudinal modes at the liquid-vapor interface are present.

III. Slosh Wave Excitation in a Partially Filled Rotating Dewar Due to Gravity Jitters

In this study, evolutions of slosh waves at the liquid-vapor interface caused by the 10-Hz gravity-jitter frequency under $10^{-4}g_0$ background gravity environment and 1.0-rpm rotating speed of the Dewar container have been investigated.

Time series of wave amplitudes for liquid-vapor interface fluctuations can be obtained from the numerical simulations of the time sequence interface oscillations accomplished in Fig. 3. Figure 4 shows the time series of wave amplitude for the liquid-vapor interface fluctuations at $z_1 = 61.46$, $z_2 = 101.4$, and $z_3 = 133.6$ cm in the axial coordinate measured from the bottom wall of the Dewar container (see Fig. 2 for the Dewar geometry).

Characteristics of slosh waves along the interface are investigated based on the data adopted from wave amplitude fluctuations at $z_1 = 61.46$, $z_2 = 101.4$, and $z_3 = 133.6$ cm in the axial coordinate measured from the bottom wall of the Dewar container, shown in Fig. 2. The wave period of various modes of slosh waves can be determined from the Fourier spectral analysis of time series at z_1, z_2, and z_3, whereas wavelength, phase velocity, and propagation direction of slosh waves can be deduced from the cross-correlation analysis of the combinations of any two time series selected out of the three time

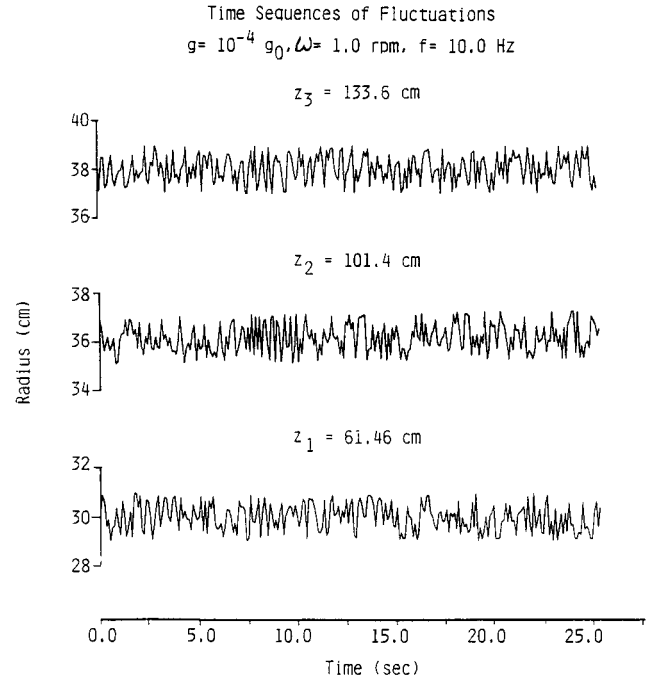

Fig. 4 Time series of wave amplitude fluctuations for the interface between liquid helium and helium vapor in a rotating propellant Dewar tank shown in Fig. 3. Three time series are detected from interfaces at $z_1 = 41.46$, $z_2 = 101.4$, and $z_3 = 133.6$ cm in the axial axis.

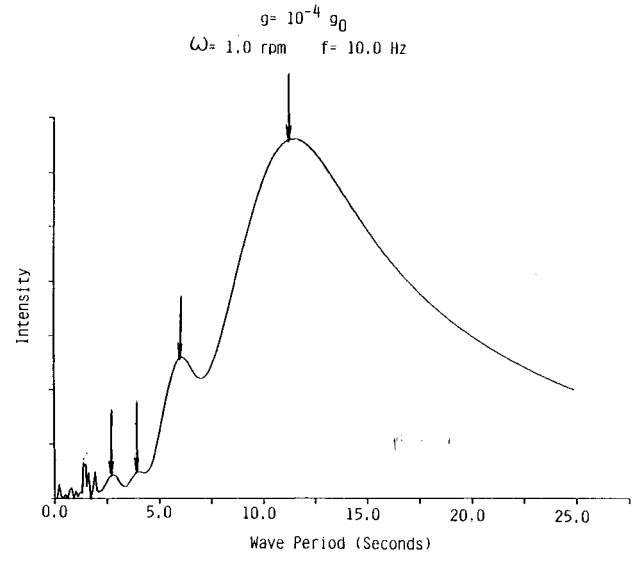

Fig. 5 Sample Fourier power spectral analysis of time series for slosh wave amplitude fluctuations under background gravity environment of $10^{-4}g_0$, rotating Dewar speed of 1.0 rpm, and gravity jitter frequency of 10 Hz, indicating four major peaks of wave modes.

series.[29-32] Figure 5 shows a sample Fourier power spectral analysis of time series at z_1. This figure clearly indicates that there are four major peaks of wave nodes corresponding to wave periods of 2.81, 4.03, 6.08, and 11.5 s. A filter shall be properly chosen to apply certain ranges of window for separating these four wave nodes, shown in Fig. 5, from each other from the data of three time series recorded at three locations, z_1 z_2, and z_3, shown in Fig. 4, for the determination of wavelength, phase velocity, and propagation direction of slosh waves.[29-32]

Table 1 shows the characteristics of major slosh waves induced by the restoring gravity jitter force fields. There are four major modes of slosh waves: two longitudinal modes with wave periods of 2.81 and 4.03 s; and two transverse

Table 1 Characteristics of major slosh waves in Gravity Probe-B Spacecraft experiment[a]

Type of wave mode	Wave period, s	Wavelength, cm	Phase velocity, cm/s	Propagation direction (clockwise from axial direction, deg)	Ratio of maximum wave amplitude to wavelength, Max (A/λ) ratio, 10^{-2}
Longitudinal	2.81	27.3	9.7	19	0.04
	4.03	41.1	10.2	23	0.03
Transverse	6.08	10.9	1.8	73	0.56
	11.5	9.2	0.8	89	1.69

[a]Background gravity = $10^{-4}g_0$; rotating speed = 1.0 rpm; frequency of gravity jitters = 10.0 Hz.

modes with wave periods of 6.08 and 11.5 s. Propagation direction (in degrees) is measured clockwise from the positive axial direction. The ratio of maximum wave amplitude to wavelength, Max (A/λ), where A is the wave amplitude and λ the wavelength of slosh wave, for each slosh wave is calculated based on the following procedures: 1) determine each wave mode based on the peaks of power intensity shown in the power spectral density analysis in the Fourier domain (see Fig. 5); 2) apply the proper window of the filter to separate each wave mode shown on the peaks of power intensity; 3) calculate wavelength, phase velocity, and propagation direction of each wave mode from the cross-correlation analysis based on the separated wave modes through filtering the time series in Fourier domain at locations z_1, z_2, and z_3; 4) reverse Fourier transform the separated wave mode based on the filtered time series in Fourier domain to time domain and obtain the amplitude of each mode of slosh waves; and 5) compute the ratio of maximum wave amplitude to wavelength [Max (A/λ)] for each mode of slosh waves from items 3 and 4.

IV. Slosh-Wave-Induced Fluid Stress Distributions on the Dewar Walls

A. Mathematical Formulation of Stress Distributions

For the purpose of considering large-amplitude slosh wave modified fluid stresses acting on the solid walls of the Dewar, the fluid stresses are decomposed into the tangential and normal components to the walls, which can be expressed as follows:

$$\Pi_t = \mu\left(\frac{\partial u_\alpha}{\partial x_\beta} + \frac{\partial u_\beta}{\partial x_\alpha}\right)\hat{t}_\alpha \hat{n}_\beta \tag{5}$$

$$\Pi_n = P\delta_{\alpha\beta} - \mu\left(\frac{\partial u_\alpha}{\partial x_\beta} + \frac{\partial u_\beta}{\partial x_\alpha}\right)\hat{n}_\alpha \hat{n}_\beta \tag{6}$$

where Π_t denotes the tangential component of fluid stresses, Π_n the normal component of fluid stresses, P the thermodynamic pressure, u_α the fluid velocity in the α direction, $\hat{t}_\alpha$ the component of unit vector tangential to the wall, and $\hat{n}_\beta$ the component of unit vector normal to the wall. Subscripts α and β imply the directions of the flowfields.

Figure 6 shows the geometry of the GP-B Dewar propellant tank. In order to make the computation of fluid stresses matching the geometry of the Dewar tank, mathematical formulations have been divided into three sections: 1) top wall (dome) section, 2) bottom wall (dome) section, and 3) cylindrical section.

Top wall (dome) section:

$$(\Pi_t)_{\text{top wall}} = \mu\left(\frac{\partial u}{\partial z} + \frac{\partial w}{\partial r}\right)\cos 2\phi \tag{7}$$

$$(\Pi_n)_{\text{top wall}} = P + \mu\left(\frac{\partial u}{\partial z} + \frac{\partial w}{\partial r}\right)\sin 2\phi \tag{8}$$

Bottom wall (dome) section:

$$(\Pi_t)_{\text{bottom wall}} = \mu\left(\frac{\partial u}{\partial z} + \frac{\partial w}{\partial r}\right)\cos 2\phi \tag{9}$$

$$(\Pi_n)_{\text{bottom wall}} = -P - \mu\left(\frac{\partial u}{\partial z} + \frac{\partial w}{\partial r}\right)\sin 2\phi \tag{10}$$

Cylindrical section:

$$(\Pi_t)_{\text{cylindrical}} = \mu\left(\frac{\partial u}{\partial z} + \frac{\partial w}{\partial r}\right) \tag{11}$$

$$(\Pi_n)_{\text{cylindrical}} = P \tag{12}$$

where ϕ is the azimuth angle of the dome. Subscripts top wall, bottom wall, and cylindrical denote stress distributions at top wall, bottom wall, and cylindrical sections, respectively. Velocity components in cylindrical coordinates of (r,θ,z) are shown as (u,v,w). As we indicated Sec. III of this paper, axial symmetric formulation is assumed in this study of slosh-wave-induced stress distribution for a partially liquid-filled rotating Dewar container. In other words, stress distribution in the circumferential direction around the axial coordinate is supposed to be symmetric, and uneven stress distribution, if any, shall

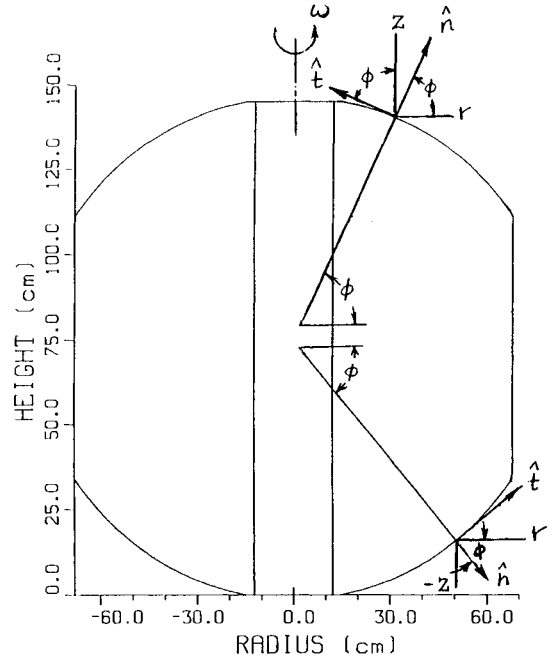

Fig. 6 Geometry of the Gravity Probe-B Spacecraft Dewar propellant tank with the coordinate system perpendicular and tangential to the surfaces of the top and bottom domes of the rotating Dewar.

be in the axial and/or radial directions of the cylindrical coordinates. To fulfill this goal, stress distributions, shown in Eqs. (7-12), must be recalculated in the axial and radial directions.

Top wall (dome) section:

$$(\Pi_{ax})_{\text{top wall}} = (\Pi_t)_{\text{top wall}} \cos\phi + (\Pi_n)_{\text{top wall}} \sin\phi$$

$$= \mu\left(\frac{\partial u}{\partial z} + \frac{\partial w}{\partial r}\right)\cos 2\phi \cdot \cos\phi + \left[P + \mu\left(\frac{\partial u}{\partial z} + \frac{\partial w}{\partial r}\right)\sin 2\phi\right]\sin\phi \quad (13)$$

$$(\Pi_{ra})_{\text{top wall}} = (\Pi_t)_{\text{top wall}} \sin\phi + (\Pi_n)_{\text{top wall}} \cos\phi$$

$$= \mu\left(\frac{\partial u}{\partial z} + \frac{\partial w}{\partial r}\right)\sin\phi \cdot \cos 2\phi + \left[P + \mu\left(\frac{\partial u}{\partial z} + \frac{\partial w}{\partial r}\right)\sin 2\phi\right]\cos\phi \quad (14)$$

Bottom wall (dome) section:

$$(\Pi_{ax})_{\text{bottom wall}} = (\Pi_t)_{\text{bottom wall}} \cos\phi - (\Pi_n)_{\text{bottom wall}} \sin\phi$$

$$= \mu\left(\frac{\partial u}{\partial z} + \frac{\partial w}{\partial r}\right)\cos 2\phi \cdot \sin 2\phi + \left[-P - \mu\left(\frac{\partial u}{\partial z} + \frac{\partial w}{\partial r}\right)\sin 2\phi\right]\sin\phi \quad (15)$$

$$(\Pi_{ra})_{\text{bottom wall}} = (\Pi_t)_{\text{bottom wall}} \sin\phi + (\Pi_n)_{\text{bottom wall}} \cos\phi$$

$$= \mu\left(\frac{\partial u}{\partial z} + \frac{\partial w}{\partial r}\right)\sin\phi \cdot \cos 2\phi + \left[-P - \mu\left(\frac{\partial u}{\partial z} + \frac{\partial w}{\partial r}\right)\sin 2\phi\right]\cos\phi \quad (16)$$

Cylindrical section:

$$(\Pi_{ax})_{\text{cylindrical}} = (\Pi_t)_{\text{cylindrical}} = \mu\left(\frac{\partial u}{\partial z} + \frac{\partial w}{\partial r}\right) \quad (17)$$

$$(\Pi_{ra})_{\text{cylindrical}} = (\Pi_\eta)_{\text{cylindrical}} = P \quad (18)$$

where Π_{ax} denotes axial components of stress, and Π_{ra} expresses radial components of stress.

Total stress and direction of stress at any location of interest can be expressed as

$$\Pi = [(\Pi_{ax})^2 + (\Pi_{ra})^2]^{1/2} \quad (19)$$

$$\phi = \tan^{-1}\left(\frac{\Pi_{ax}}{\Pi_{ra}}\right) \quad (20)$$

In this study, flowfields of a partially liquid filled rotating Dewar have been numerically computed and shown in the first paper. With the computed results of P, $\partial u/\partial z$, and $\partial w/\partial r$ at each grid point along the wall, one can seek stress distributions at every location along internal and external walls of the rotating Dewar tank.

B. Slosh Wave Induced Fluid Stress Distributions

Fluid stress distribution at the interfaces of liquid-solid, vapor-solid, and liquid-vapor under the dynamical impact of slosh wave excitation can be computed. In this study, we are particularly interested in the fluid (liquid and vapor) stresses exerted on the solid walls of the Dewar container, including the outer and inner walls. Figure 6 shows that the outer wall contains three sections (top dome, cylindrical, and bottom dome), whereas the inner wall is in a profile of the cylinder.

By combining axial and radial components of fluid stress distribution at the top dome, the cylindrical, and the bottom dome, shown in Eqs. (13-18), one can compute the magnitude and direction of total stress distribution exerted on the outer wall of the Dewar, as shown in Eqs. (19) and (20). The inner wall fluid stress distribution can be calculated based on the cylindrical section formulation, shown in Eqs. (17-20).

Figure 7 shows time sequence distributions of fluid stresses exerted on the outer wall, and Fig. 8 illustrates time sequence distributions of fluid stresses exerted on the inner wall. In these figures, solid lines show the magnitude of fluid stresses in units of dyne/cm^2 (scale shown on the lower side of the horizontal axis), the dotted lines illustrate the direction of fluid stress (scale shown on the upper side of the horizontal axis with positive angle indicating upward direction; negative angle, the downward direction; and zero angle, the horizontal direction). In these figures, the vertical axis shows the values at the corresponding location of the axial coordinate measured from the bottom wall of the Dewar. Vapor pressure of helium keeps the saturation vapor pressure at 1.8 K, which is 16,625 dyne/cm^2, or 12.47 Torr.

Figure 7 shows time sequence evolution of fluid stress distribution exerted on the outer wall at a background environment of $10^{-4}g_0$, Dewar rotating speed of 1.0 rpm, with gravity jitter frequency of 10 Hz. The dynamics of bubble interface shows a configuration of a vertically elongated doughnut with a near conical shape cross section attached to the upper central section around the inner wall of the rotating Dewar with oscillations imposed by a series of slosh wave propagation (see Fig. 3 for the time evolution of interface oscillations, and Fig. 4 for time sequences of fluctuations). Characteristics of slosh waves are illustrated in Table 1. It is shown in Fig. 7 that there are

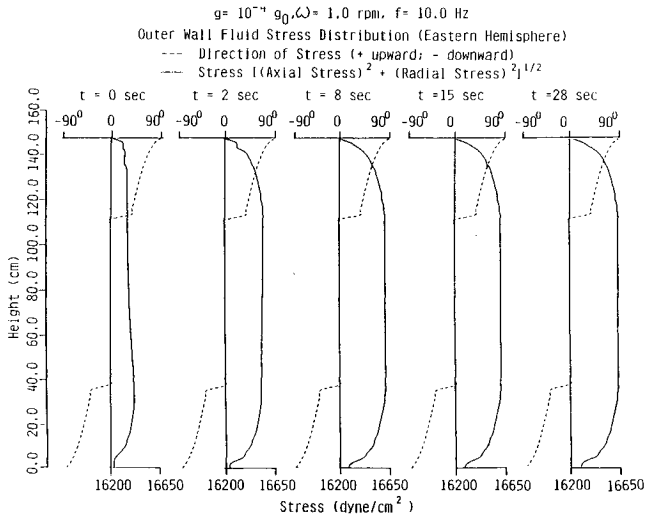

Fig. 7 Time evolution of slosh wave disturbance-associated fluid stress distribution exerted on the outer wall at the eastern hemisphere section of the Dewar under the conditions of background gravity level = $10^{-4}g_0$, rotating speed = 1.0 rpm, and gravity jitter frequency = 10 Hz.

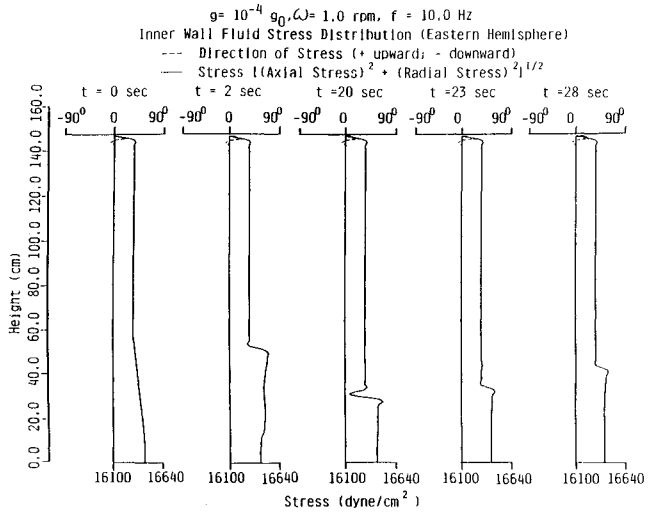

Fig. 8 Time evolution of slosh wave disturbance-associated fluid stress distribution exerted on the inner wall at the eastern hemisphere section of the Dewar under the conditions of background gravity level = $10^{-4}g_0$, rotating speed = 1.0 rpm, and gravity jitter frequency = 10 Hz.

time-dependent fluctuations of fluid stress distribution at the upper top dome section of the outer wall of the Dewar tank caused by the slosh wave associated oscillations of bubble interface that appeared in the top dome section. As to the cylindrical and bottom dome sections, it shows time-dependent oscillations of fluid distribution. It is also obvious that the maximum fluid stress distributions are always located in the upper cylindrical section near the top dome of the outer wall in this case.

Comparing Figs. 3 and 7, they show that the locations of maximum fluid stress distribution always correspond to the nearby locations of slosh wave excitations along the liquid-vapor interface with maximum wave amplitude oscillations. This result indicates that the fluctuations of torque exerted on the spacecraft Dewar tank are closely related to the slosh wave excitations.

Figure 8 shows the time sequence evolution of fluid stress distribution exerted on the inner wall of the rotating Dewar. In view of Fig. 3 for flow profiles around the inner wall of the Dewar container it shows that there was no liquid helium attached on the upper half section of the inner wall, whereas the liquid helium attached on the lower half section of the inner wall was deeply influenced by the circulation flow patterns induced by the large-amplitude fluctuations of slosh waves propagated along the liquid-vapor interface. These results were reflected on the fluid stress distributions on the inner wall in which there were dramatic time-dependent fluctuations in the liquid-attached section of fluid stress distribution exerted on the lower section of the inner wall in this case. In comparison of fluid stress distribution exerted between the inner and outer walls, it also shows that the contribution on the outer wall is much greater than that on the inner wall due to the effect of centrifugal force.

V. Conclusions

The time evolutions of slosh-wave-induced fluid stress distribution exerted on the outer and inner walls of a rotating Dewar have been studied. Results show that fluid stress distribution exerted on the outer wall is always greater than that exerted on the inner wall (see Figs. 7 and 8). It also shows that there are time-dependent fluctuations of the fluid stress distribution at the top dome and upper cylindrical sections of the outer wall that are dependent on the location of the liquid-vapor interface. These fluctuations excite large-amplitude slosh waves that disturb the entire flowfield within the rotating Dewar (see Fig. 3 for interface disturbances, and Fig. 4 for time sequence fluctuations). A computer algorithm has been demonstrated that can be used to simulate the fluid behavior in a microgravity environment, in particular, the production of uneven distributions in fluid stress exerted on the Dewar walls. In GP-B Spacecraft, the goals of the experiments are to find distinct space-time processes, frame dragging (measuring the rotation of space-time) and the geodetic effect (measuring the curvature of space-time), which require the high degree of drag-free operation. The present study can greatly contribute to these goals by proper control of torque and angular momentum disturbances caused by large-amplitude slosh wave excitation and fluid stress distribution exerted on the Dewar. The results obtained should be useful in handling and managing the cyrogenic liquid propellant and in designing the attitude control spacecraft that contain large amounts of cryogenic liquids.

Acknowledgment

The authors appreciate the support received from NASA through Grants NAG8-035 and NAG8-129. The authors would like to express their gratitude to Richard A. Potter of NASA Marshall Space Flight Center for the stimulating discussions during the course of the present study.

References

[1]Wilkinson, D. T., et al., "Gravitation, Cosmology and Cosmic-Ray Physics," *Physics Today,* Vol. 39, No. 1, 1986, pp. 43-46.

[2]Everitt, F., "Stanford Relativity Gyroscope Experiment (NASA Gravity Probe B)," *Proceedings of the Society of Photo-Optical Instrumentation Engineers,* Vol. 619, 1986, pp. 1-165.

[3]Hung, R. J., and Leslie, F. W., "Bubble Shapes in a Liquid-Filled Rotating Container Under Low Gravity," *Journal of Spacecraft and Rockets,* Vol. 25, No. 1, 1988, pp. 70-74.

[4]Hung, R. J., Tsao, Y. D., Hong, B. B., and Leslie, F. W., "Bubble Behaviors in a Slowly Rotating Helium Dewar in Gravity Probe-B Spacecraft Experiment," *Journal of Spacecraft and Rockets,* Vol. 26, No. 3, 1988, pp. 167-172.

[5]Hung, R. J., Tsao, Y. D., Hong, B. B., and Leslie, F. W., "Dynamical Behavior of Surface Tension on Rotating Fluids in Low and Microgravity Environments," *International Journal for Microgravity Research and Applications,* Vol. 2, No. 1, 1989, pp. 81-85.

[6]Leslie, F. W., "Measurements of Rotating Bubble Shapes in a Low Gravity Environment," *Journal of Fluid Mechanics,* Vol. 16, No. 2, 1985, pp. 269-279.

[7]Kitchens, C. W., Jr. "Navier-Stokes Equations for Spin-Up in a Filled Cylinder," *AIAA Journal,* Vol. 18, No. 8, 1980, pp. 929-934.

[8]Veldman, A. E. P., and Vogels, M. E. S., "Axisymmetric Liquid Sloshing Under Low Gravity Conditions," *Acta Astronautica,* Vol. 11, No. 4, 1984, pp. 641-649.

[9]Homicz, G. F., and Gerber, N., "Numerical Model for Fluid Spin-Up from Rest in a Partially Filled Cylinder," *Journal of Fluids Engineering,* Vol. 109, No. 1, 1987, pp. 194-197.

[10]Karotani, Y., Prasad, A., and Oastrach, S., "Thermal Convections in an Enclosure Due to Vibrations Aboard a Spacecraft," *AIAA Journal,* Vol. 19, No. 3, 1981, pp. 511-516.

[11]Hung, R. J., Lee, C. C., and Shyu, K. L., "Reorientation of Rotating Fluid in Microgravity Environment With and Without Gravity Jitters," *Journal of Spacecraft and Rockets,* Vol. 28, No. 1, 1991, pp. 71-78.

[12]Hung, R. J., Tsao, Y. D., Hong, B. B., and Leslie, F. W., "Time Dependent Dynamical Behavior of Surface Tension on Rotating Fluids Under Microgravity Environment," *Advances in Space Research,* Vol. 8, No. 12, 1989, pp. 205-213.

[13]NASA Office of Aeronautics and Space Technology, *Technology for Future NASA Missions: Civil Space Technology Initiative and Pathfinder,* NASA CP-3016, 1988, pp. 568.

[14]Hung, R. J., Tsao, Y. D., Hong, B. B., and Leslie, F. W., "Axisymmetric Bubble Profiles in a Slowly Rotating Helium Dewar Under Low and Microgravity Environments," *Acta Astronautica,* Vol. 19, No. 3, 1989, pp. 411-426.

[15] Hung, R. J., Lee, C. C., and Leslie, F. W., "Effect of G-Jitters on the Stability of Rotating Bubble Under Microgravity Environment," *Acta Astronautica,* Vol. 21, No. 2, 1990, pp. 309-321.

[16]Hung, R. J., Lee, C. C., and Leslie, F. W., "Response of Gravity Level Fluctuations on the Gravity Probe-B Spacecraft Propellant System," *Journal of Propulsion and Power,* Vol. 7, No. 4, 1991, pp.

556-564.

[17]Hung, R. J., and Shyu, K. L., "Cryogenic Liquid Hydrogen Reorientation Activated by High Frequency Impulsive Reverse Gravity Acceleration of Geyser Initiation," *Microgravity Quarterly,* Vol. 1, No. 2, 1991, pp. 81-92.

[18]Hung, R. J., and Shyu, K. L., "Constant Reverse Thrust Activated Reorientation of Liquid Hydrogen with Geyser Initiation," *Journal of Spacecraft and Rockets,* Vol. 29, No. 2, 1992, pp. 279-285.

[19]Hung, R. J., Shyu, K. L., and Lee, C. C., "Slosh Wave Excitation Associated with High Frequency Impulsive Reverse Gravity Acceleration of Geyser Initiation," *Microgravity Quarterly,* Vol. 1, No. 3, 1991, pp. 125-133.

[20]Hung, R. J., Shyu, K. L., and Lee, C. C., "Liquid Hydrogen Slosh Wave Excited by Constant Reverse Gravity Acceleration of Geyser Initiation," *Journal of Spacecraft and Rockets* (to be published).

[21]Hung, R. J, Lee, C. C. and Leslie, F. W., "Slosh Wave Excitation in a Partially Filled Rotating Tank Due to Gravity Jitters in a Microgravity Environment," *Acta Astronautica,* Vol. 25, No. 3, 1991, pp. 523-551.

[22]Hung, R. J., and Shyu, K. L., "Space-Based Cryogenic Liquid Hydrogen Reorientation Activated by Low Frequency Impulsive Reverse Gravity Thruster of Geyser Initiation," *Acta Astronautica,* Vol. 25, No. 4, 1991, pp. 709-719.

[23]Mason P., Collins, D., Petrac, D., Yang, L., Edeskuty, F., Schuch, A., and Williamson, K., "The Behavior of Superfluid Helium in Zero Gravity," *Proceedings of the 7th International Cryogenic Engineering Conference,* Science and Technology Press, Surrey, England, UK, 1978.

[24]Hung, R. J., "Superfluid and Normal Fluid Helium II in a Rotating Tank Under Low and Microgravity Environments," *Proceedings of the National Science Council, Series (A),* Vol. 14, No. 2, 1990, pp. 289-297.

[25]Harlow, F. H., and Welch, J. E., "Numerical Calculation of Time-Dependent Viscous Incompressible Flow of Fluid with Free Surface," *Physics of Fluids,* Vol. 8, No. 10, 1965, pp. 2182-2193.

[26]Spalding, D. B., "A Novel Finite-Difference Formulation for Differential Expressions Involving Both First and Second Derivatives," *International Journal of Numerical Methods in Engineering,* Vol. 4, No. 3, 1972, pp. 551-563.

[27]Patankar, S. V., *Numerical Heat Transfer and Fluid Flow,* Hemisphere-McGraw-Hill, New York, 1980, pp. 197.

[28]Patankar, S. V., "A Calculation Procedure for Heat, Mass and Momentum Transfer in Three Dimensional Parabolic Flows," *International Journal of Heat and Mass Transfer,* Vol. 15, No. 1, 1972, pp. 15-24.

[29]Hung, R. J., Phan, T., and Smith, R. E., "Observation of Gravity Waves During the Extreme Tornado Outbreak of April 3, 1974." *Journal of Atmospheric and Terrestrial Physics,* Vol. 40, No. 4, 1978, pp. 831-843.

[30]Hung, R. J., and Smith, R. E., "Ray Tracing of Gravity Waves as a Possible Warning System for Tornadic Storms and Hurricanes," *Journal of Applied Meteorology,* Vol. 17, No. 1, 1978, pp. 3-11.

[31]Hung, R. J., and Kuo, J. P., "Ionospheric Observation of Gravity Waves Associated with Hurricane Eloise," *Journal of Geophysics,* Vol. 45, No. 1, 1978, pp. 67-80.

[32]Hung, R. J., Phan, T., and Smith, R. E., "Coupling of Ionosphere and Troposphere During the Occurence of Isolated Tornados of November 20, 1973," *Journal of Geophysical Research,* Vol. 84, No. 5, 1979, pp. 1261-1268.